*Article*

# A Preliminary Assessment of Underground Space Resources for Hydrogen Storage in Salt Caverns in Lambton County, Southern Ontario, Canada

Ling Li [1,2,3], Shunde Yin [3,*] and Zhizhang Wang [1,2]

1    State Key Laboratory of Petroleum Resources and Prospecting, China University of Petroleum-Beijing, Beijing 102249, China; sevendel@163.com (L.L.)
2    College of Geosciences, China University of Petroleum-Beijing, Beijing 102249, China
3    Department of Civil and Environmental Engineering, University of Waterloo, Waterloo, ON N2l 3Gl, Canada
*    Correspondence: shunde.yin@uwaterloo.ca

**Abstract:** Underground hydrogen storage (UHS) is considered to solve the intermittency problem of renewable energy. A geological assessment indicated that the B unit of the Salina Group in Southern Ontario, Canada, is the most promising for UHS because it is the thickest and most regionally extensive salt rock deposit. However, the comprehensive geological knowledge of potential sites and overall salt volume for UHS remains undiscovered. This paper collected 1112 wells' logging data to assess the geologic potential for UHS in Lambton County. The geological characteristic analysis of the B unit was conducted using high-frequency stratigraphic sequences and logging interpretation. The internal lithologies and thicknesses of the B unit were interpreted from 426 available wells. The storage capacity of the salt caverns was calculated from simplified cylinder models. The results indicate that the B unit can be subdivided into three high-frequency sequences, denoted as the SQ1, SQ2, and SQ3 subunits. SQ1 corresponds to salt–limestone, SQ2 corresponds to bedded salt rocks, and SQ3 corresponds to massive salt rocks. Well sections and thickness maps indicate that the study area can be divided into two sub-areas along the Wilikesport, Oil Spring, and Watford line. To the northwest, unit B was thicker and deeper in terms of paleo-water depth, and to the southeast, less of the B unit was deposited on the paleo-highs. The main thicknesses in SQ1, SQ2, and SQ3 range from 20 to 30 m, 25 to 35 m, and 30 to 40 m, respectively. In conclusion, the best subunit for UHS is SQ3, with a secondary target being SQ2. The main factor impacting cavern storage capacity for the SQ2 subunit is high mud content, while for SQ3, it is the meters-thick anhydrite developed towards the base of the unit. The available underground storage volume of the salt caverns in the B unit is $9.10 \times 10^6$ m$^3$. At the standard state, the working gas volume is $557.80 \times 10^6$ m$^3$. The favorable area for UHS is the western part surrounded by Wallaceburg, Oil Spring, and Watford. The thickness distribution of the B unit is the combined result of paleo-topography, sea-level changes, and tectonic movement in Lambton. The geological storage capacity of the salt caverns exhibits significant potential.

**Keywords:** renewable energy; energy storage; underground hydrogen storage; salt caverns

## 1. Introduction

An effective means to reduce carbon dioxide emissions altering the global climate is the use of environmentally friendly renewable energy sources [1]. However, wind and solar energy, among these sources, are intermittent and dependent on seasonal and weather conditions. Addressing this intermittency is crucial [2]. The key to addressing this challenge is energy storage, with various storage technologies currently being developed and refined. Based on the forms of energy storage, six storage systems can be categorized: thermal

energy storage, mechanical energy storage, chemical energy storage, electrochemical energy storage, electrical energy storage, and other types of energy storage systems. Among these, chemical energy storage systems are particularly well suited for long-term storage [3]. The energy is stored within the chemical bonds between the atoms and molecules of the energy carrier, and subsequently released during chemical reactions. Hydrogen energy storage, a form of chemical energy storage, offers a promising solution to address the intermittency issue of renewable energy. Hydrogen, a green energy carrier, can be directly generated from water and produces electricity without carbon emission. Research on production, storage, transportation, and utilization of hydrogen is ongoing [4–13]. Hydrogen molecules readily react with the storage medium, imposing stringent requirements on hydrogen storage materials. However, rocks exhibit lower reactivity with hydrogen and can serve effectively as a storage medium [14,15]. Among storage strategies, underground hydrogen storage (UHS) offers the advantages of safety, economic viability, large capacity, and small surface footprint over above-ground hydrogen storage [8,16,17].

Depleted oil and gas reservoirs, aquifers, and salt caverns have been considered candidates for geologic UHS, with salt caverns being ideal due to their chemical inertness and excellent sealing performance [8,16]. Currently, there are four high-purity hydrogen storage sites and one medium-purity site operational worldwide (Figure 1a,b). Specifically, shallowly buried salt caverns are located in the UK and Texas, USA [8]. In Europe, geological assessments of salt caverns are widely conducted, and potential sites have been identified (Figure 1a). Germany benefits from favorable geological conditions for implementing hydrogen storage in salt caverns, and significant research has been conducted on UHS [13,17–20]. Three trap types identified from a structural geological model are targeted as potential hydrogen storage sites in the North German Basin [13]. In Poland, detailed assessments of hydrogen storage potential have been conducted in both bedded salt formations and salt domes, resulting in more accurate forecasts of rock salt deposit capacity for hydrogen storage [21,22]. Indeed, various potential salt cavern sites worldwide have been documented, including in Southern Ontario, Canada [8] (Figure 1c). The purity of salt rock, along with the form and thickness of deposit units, are critical geological factors influencing the potential for UHS in bedded salt rock formations in Canada [23]. Geological assessment is a crucial step towards the commercialization of UHS, necessitating analysis of the depth, deposit unit types, structure, and lithology or purity of salt rocks.

Ontario possesses abundant energy resources and has been exporting energy for decades. Southern Ontario primarily hosts significant renewable energy sources like solar and wind energy. In 2022, these renewable energy systems generated $52.38 \times 10^3$ GJ of energy [24]. The distribution of wind farms in Ontario coincides geographically with the underground salt rock units and depleted gas reservoirs, particularly in Lambton County for salt caverns. Excess renewable energy in the form of electricity can be used to generate hydrogen, which is then stored underground for use during peak hours. Geological hydrogen storage mitigates the intermittency of renewable energy, contributing to the achievement of net zero carbon emissions. Beyond energy consumption, hydrogen can also be utilized for medical, industrial, and other purposes [25–27]. Significant hydrogen storage capacity not only meets energy demands but also supports applications across various sectors, advancing the hydrogen economy. UHS will drive the development of a comprehensive hydrogen economy focused on hydrogen utilization (Figure 2).

Geological assessments of Lambton have identified the B and A2 unit successions containing salt rock, developed in the shallow evaporite Salina Group (Table 1) [28].

**Table 1.** The lithology of the thickness of each unit in Ontario (modified from [29,30]).

| Formation | | | Gamma | Lithology | Depth (m) | Unit | Description |
|---|---|---|---|---|---|---|---|
| Mississippian | | | | | | G unit | Fine crystalline brown dolostone, shaly dolomite, some anhydrite, red |
| Devonian | Upper | | | | | F unit | Salt, in thick beds separated by beds of shale, shaly dolostone, grey and buff and brown crystalline dolostone; anhydrite nearly always present. |
| | Middle | | | | 200 | F salt | |
| | Lower | | | | 400 | E unit | Thin shale unit, argillaceous grey and buff dolostone. |
| Silurian | Upper | | | Salt | | D unit | Salt, nearly pure; minor, thin dolostone and shale beds. |
| | | | | | 600 | C unit | Lower bed of shaly anhydrite or dolostone, grading upwards to green shale with anhydrite nodules. |
| | | | | | | B unit | |
| | | | | | 800 | B salt | Salt, in thick salt beds with thin shale or dolostone interbeds. The base of the B unit is marked by an anhydrite-rich zone. |
| | Lower | | | | 1000 | | |
| Ordovician | Upper | | | Shale | | A2 carbonate | Dark to light grey-brown, laminated to thin-bedded, very fine- to fine-grained dolostone and limestone. |
| | | | | | 1200 | A2 evaporatie | Salt up to 45 meters thick; where salt is absent, the base is marked by anhydrite. |
| | Middle | | | Carbonate | 1400 | A1 carbonate | Very fine- to medium-grained, tan-grey to black, variably bituminous, laminated to massive dolostone and limestone. |
| | | | | | | A1 anhydrite | Anhydrite with minor dolostone and salt. |
| Upper Cambrian | | | | Sandstone | | A0 carbonate | Dark brown to black, laminated, bituminous dolostone. |

The A2 unit consists of salt rocks that contain carbonate rocks, which are not suitable for long-term storage [31], while the B unit consists of salt rocks with an average thickness of 90 m and an average depth of around 400 m below the surface; the B unit has been considered the most promising option for UHS. However, due to the lack of geological characterization of the internal subunits and lateral variations in the thickness of the B unit in Lambton, there is a knowledge gap regarding the overall salt volume and its spatial variation for UHS.
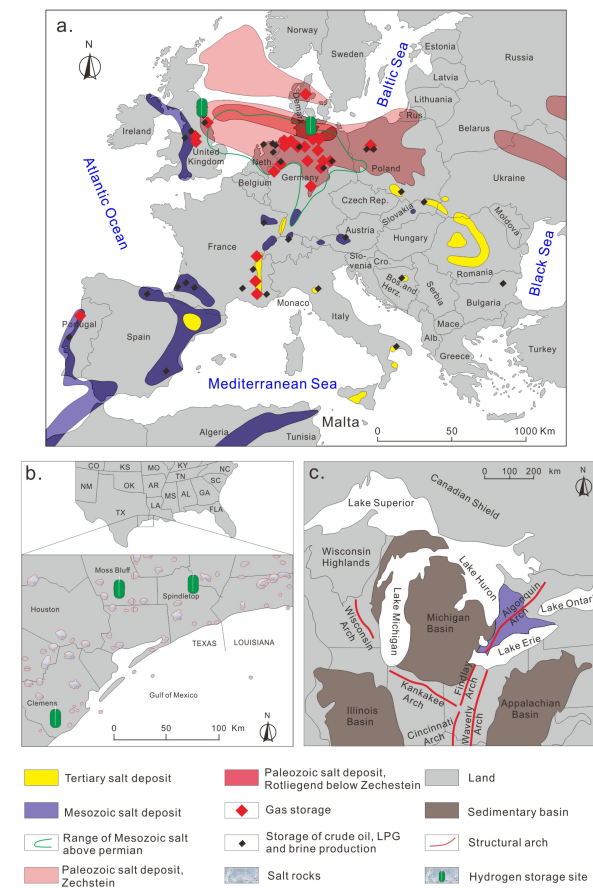


**Figure 1.** The distribution of salt deposits and salt rock hydrogen storage sites in the world (modified from [8,32,33]). (**a**) The salt deposit distribution in Europe [32]. (**b**) The salt deposit distribution in Texas, USA [8]. (**c**) The salt deposit distribution in Southern Ontario, Canada [33].
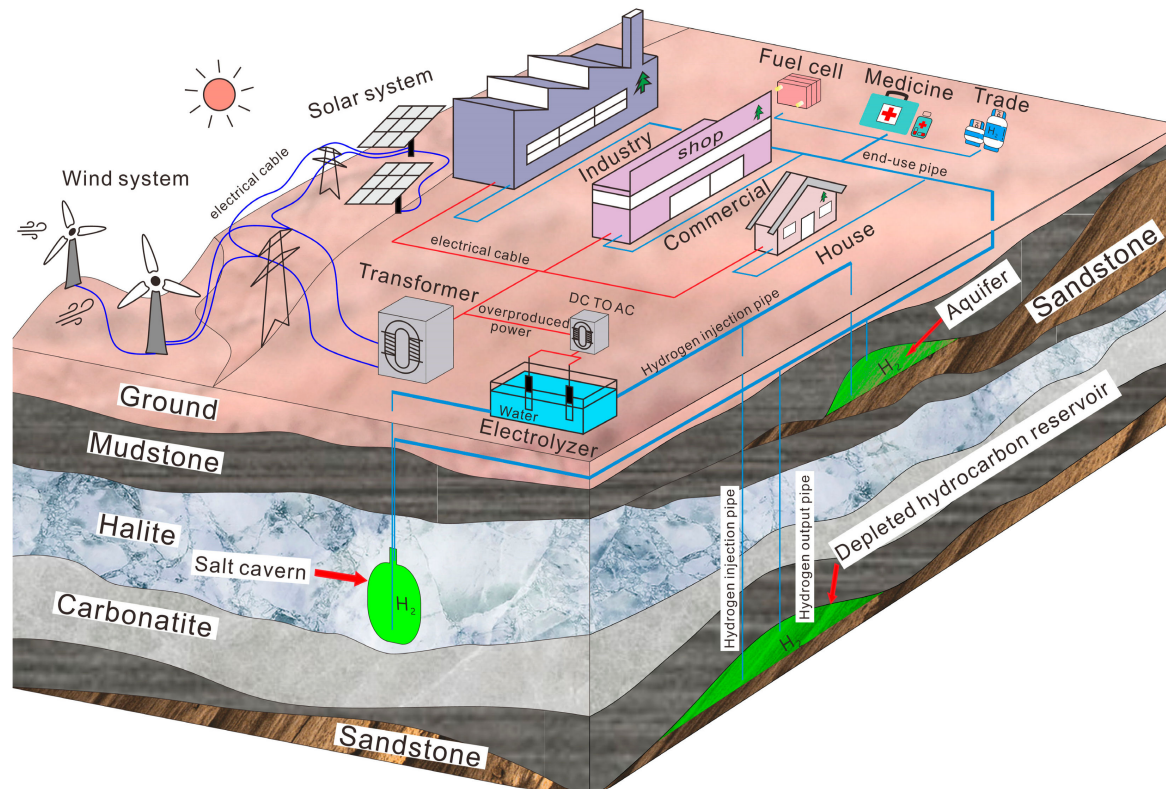
**Figure 2.** The comprehensive hydrogen economy concept model of UHS.

To address this knowledge gap, this study collected data from 1112 wells and interpreted 426 wells in Lambton to document the internal subunits, lithologies, form, and thickness of the B unit of the Salina Group in Southern Ontario. The geological storage potential of the salt cavern was quantitatively assessed in Lambton, promoting the commercialization of UHS. In the rest of this paper, three internal high-frequency sequences are identified based on the characteristics of logging curves and the concept of high-frequency sequence stratigraphy. The form and thickness distributions of three high-frequency sequence subunits are presented to highlight favorable areas for UHS. The volumes of storage space within hydrogen gas are also assessed.

## 2. Geological Setting

Lambton is situated within the tectonically stable interior of the North American Craton on the southeastern margin of the bowl-shaped Paleozoic Michigan Basin in Southern Ontario, Canada (Figure 3) [34]. The depositional environment of the Michigan Basin changed due to the horizontal and vertical loading being affected by the far-field tectonics associated with the Taconic and Acadian orogenies during the Paleozoic [35]. In the Upper Silurian, the Michigan Basin became a restricted marine basin that experienced extreme sea-level oscillations, leading to hypersaline conditions and the formation of the Salina Group [34]. During the Silurian Period, the Michigan Basin covered what are now parts of Michigan, Wisconsin, and Ontario.

The Salina Group hosts one of the most extensive and well-known salt deposits in the world [34], formed by multiple marine transgressive events [36]. This succession consists of up to 420 m of evaporitic carbonates, shales, and evaporites, in Sarnia, Southern Ontario, and is up to 750 m thick in the center of the Michigan Basin [29]. The Salina Group is informally subdivided and named from A- to G-lettered units, with each subunit distinguished by lithology corresponding to the 3rd- or 4th-order sequence boundaries [34]. The lithologies of these evaporite units are influenced by the evolution of eustasy, with carbonate deposited during

the sea-level rising period and evaporite deposited during the sea-level falling period [34,37]. The detailed lithology and the thickness of each unit are listed in Table 1.
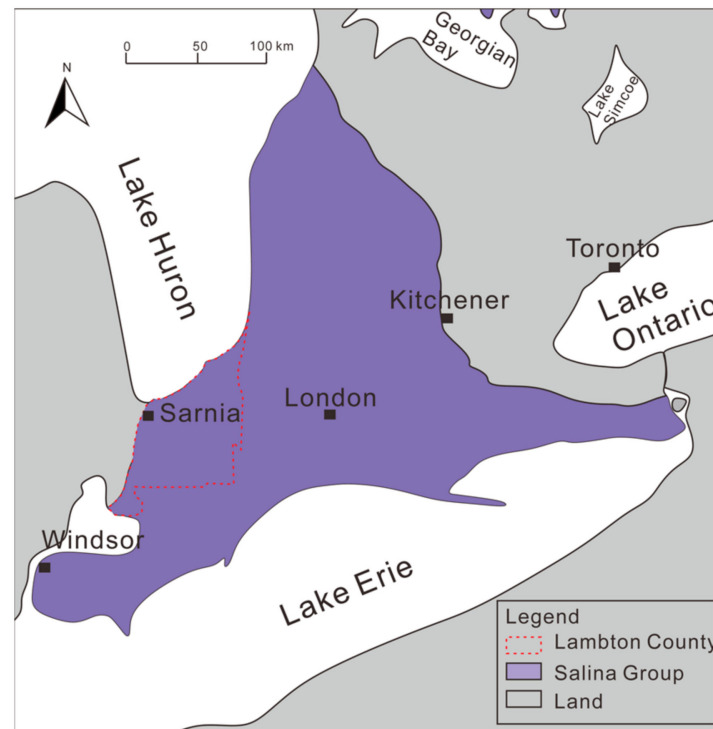


**Figure 3.** Locations in and lithostratigraphy of Lambton, Southern Ontario.

Unit A contains two evaporite cycles, "A-1" and "A-2", and three carbonate interbeds, "A-0", "A-1", and "A-2". Unit B is an evaporite unit widely distributed in the basin, except for the southern margin. It can be subdivided into several fine cycles, with its thickness ranging from 145 m in the basin center to less than 15 m at the margins, affected by pinching out and changing to anhydrite in the lower halite member [38]. The B unit mainly occurs in the basin center to the north of the margin, at subsurface depths between 275 m and 825 m in Ontario. Salt rock and shale are two main lithologies. Shale resulted from sea-level rises, while salt rock formed during sea-level falls [39].

## 3. Methods

Data were collected from 1112 wells, and included drawings and logs. Internal high-frequency sequence subunit subdivision and lithology interpretation were conducted on 426 wells using *Reform* software. The thicknesses of three high-frequency sequence sub-units within the B unit were mapped to identify potentially favorable areas for UHS. Additionally, paleo-water depth maps were constructed to investigate the spatial heterogeneity of these subunits. Finally, the storage capacity of salt caverns was calculated based on 426 wells with confirmed lithology and thickness.

### 3.1. Lithology and Stratigraphy

The lithology identification of internal units in this paper adopts the evaporite geological log analysis method of the Kansas Geological Survey, USA (Figure 4) [40]. The highly distinctive petrophysical properties of shale and evaporite make them easy to recognize on a standard log suite. Shale shows high natural radiation and porosity readings in logging data, while evaporite exhibits the opposite characteristics. Hydrogen storage-capable salt caverns can exclusively originate from halite within evaporite formations that is water-soluble. The types of the salt rock vary and are related to the sequence units [41].
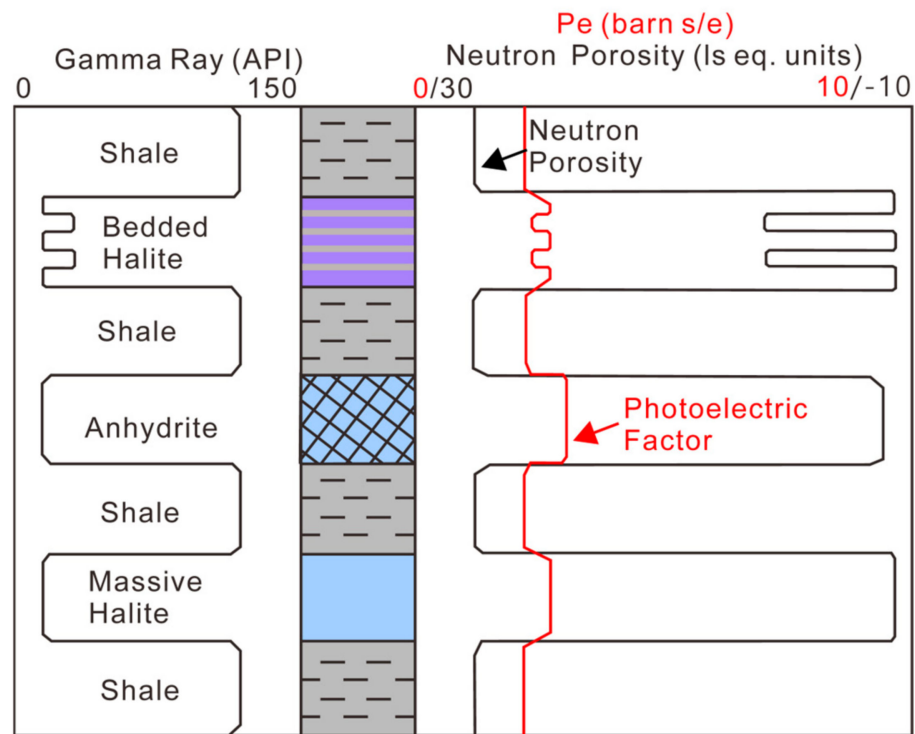
**Figure 4.** The log corresponding to marine evaporites modified from [40].

The sequence subdivision of unit B refers to high-frequency sequence stratigraphy methods based on well logging data [41]. The high-frequency sequence boundaries correspond to flooding surfaces, which highlight the cyclic sedimentary units of evaporites and are generally identified using gamma ray (GR) logging data (Figure 5). The trend of GR curves also reflects the variation in shale content (insoluble content). The high-frequency stratigraphy model was applied to the B unit to study vertical lithological and horizontal succession changes.
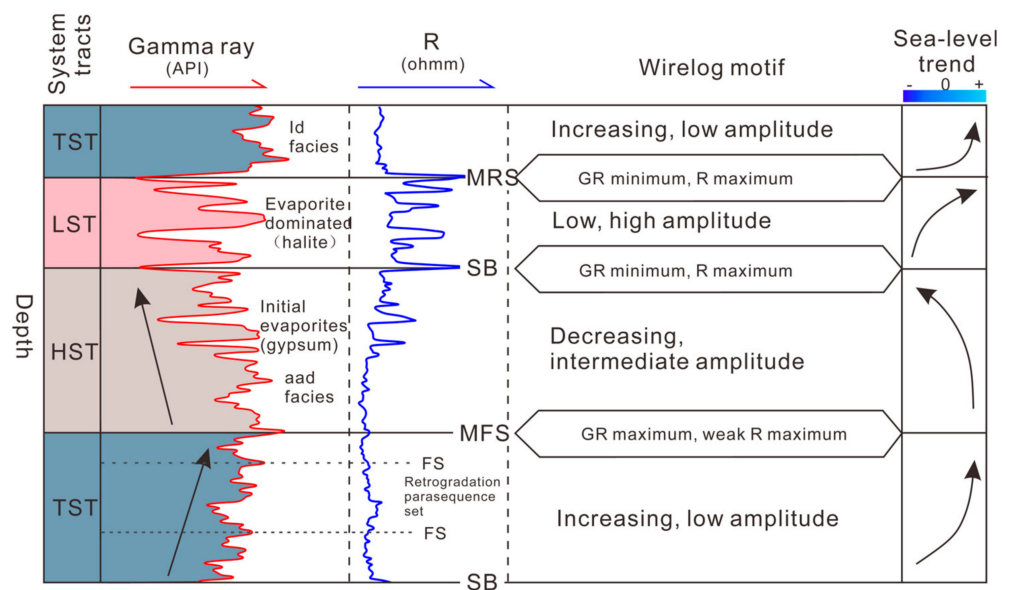


**Figure 5.** The log corresponding to evaporite sequence surfaces in the sequence stratigraphic model modified from [41]. TST: transgressive system tract, HST: high stand system tract, LST: low stand system tract, SB: shelf beak, MFS: maximum flooding surface, TS: transgression surface, FS: flooding surface. MRS: maximum regressive surface.

### 3.2. Storage Capacity of Salt Cavern

Due to the lack of spatial constraints from seismic data, the strata model based on wells is rough and has low accuracy. To conduct a reliable assessment, it is assumed that all 426 wells are available for forming caverns. Hydrogen storage-capable salt caverns are manufactured and require water-soluble halite within evaporite formations. The geometry of the caverns can be approximated as a cylinder. Thus, the calculation of the storage space of the cavern is guided by the simplified concept of the cylinder model [22]. The storage volume of the cylinder follows as (1):

$$V_{cyli} = \pi * r_{salt}^2 * H_{salt} \tag{1}$$

where $V_{cyli}$ is the underground storage volume of the salt cavern, $\pi$ is pi as 3.14, $r_{salt}$ is the radius of the salt rock cavern, and $H_{salt}$ is the height of the cavern.

The cylinder model necessitates that the salt rock thickness exceeds 30 m, with minimum salt thicknesses of the roof and floor of 20 and 10 m, respectively [42,43]. The height is determined by subtracting 30 from the salt rock succession. The radius is taken as half of the height to ensure the stability of the cavern and maximize storage capacity [30]. Considering economic conditions, the thickness requirement for the cavern succession should substantially exceed 30 m.

A perfect cylinder cannot form in solution-mined caverns, especially in salt rock successions containing shale, which affects the development of the caverns, resulting in a rough cylinder. Shape correction factors should be applied to the cavern volume estimates, with a factor of 0.7 being acceptable in volume calculation [43]. Additionally, the insoluble content in evaporative rocks reduces the volumes of caverns. The average 15% insoluble content is acceptable. The corrected cavern storage volume is as shown in Equation (2):

$$V_{cav} = V_{cyli} * f_{shape} * (1 - p_{inso}) \tag{2}$$

where $V_{cav}$ is the underground volume of the salt cavern, $f_{shape}$ is the shape correction factor as 0.7, and $p_{inso}$ is the average insoluble content of the salt rock as 15%.

### 3.3. The Volume of Compressed Gas

Pressure and temperature are two parameters involved in calculating the underground total compressed gas storage volume. The internal pressure of the cavern is equal to the lithostatic pressure at the middle of the cavern. The average density of the succession above the salt cavern is estimated as 2.3 g/cm$^3$, and the approximate calculation of storage cavern pressure is based on Equation (3):

$$P_{lithostatic} = \rho * g * (D_{salt} + H_{salt}/2) \tag{3}$$

where $P_{lithostatic}$ is the lithostatic pressure, $\rho$ is the average density of the overlying succession, $D_{salt}$ is the depth of the salt cavern, $H_{salt}$ is the height of the salt cavern, and g is the gravity acceleration (9.8 m/s$^2$).

The temperature is estimated according to Equation (4):

$$T_m = T_0 + T_{grad} * (D_{salt} + H_{salt}/2) \tag{4}$$

where $T_0$ is the surface temperature, $T_{grad}$ is the gradient of the temperature with depth, $D_{salt}$ is the depth of the salt cavern, and $H_{salt}$ is the height of the salt cavern. The Michigan Basin geothermal gradient of 25 °C/km was taken.

The total stored gas consists of energy storage gas and cushion gas. Cushion gas is permanently stored to maintain the geomechanical stability of the cavern [44]. The energy storage gas is the hydrogen gas, but not all of it can be decompressed. Only working gas can be used for injection and decompression. This is calculated based on the minimum and maximum operating pressures for a salt cavern, which are 30% and 80% of the lithostatic

pressure, respectively [42,45]. The underground hydrogen working gas pressure is shown as Equations (5) and (6):

$$P_{minworking} = P_{lithostatic} * 30\% \tag{5}$$

$$P_{maxworking} = P_{lithostatic} * 80\% \tag{6}$$

where $P_{minworking}$ is the minimum underground hydrogen working gas pressure and $P_{maxworking}$ is the maximum underground hydrogen working gas pressure.

Then, underground storage volume is converted into the standard state volume according to Equation (7):

$$V_g = V_{cav} * \left( \left( P_{maxworking} - P_{minworking} \right) / P_g \right) * \left( T_g / T_m \right) \tag{7}$$

where $V_g$ is the ground storage volume at the standard state, $V_{cav}$ is the underground storage volume of the salt cavern, $P_g$ is the standard state of pressure as 101.3 kPa, and $T_g$ is the standard state temperature as 0 °C. $P_{working}$ is the underground salt cavern pressure. $T_m$ is the estimated temperature of the salt cavern.

## 4. Subdivision of Salt Unit in Lambton County

### 4.1. Basic Geological Settings in Lambton County

The burial depth of the B unit ranges from 160 to 480 m in Lambton, Southern Ontario (Figure 6a). The thicker salt rock is predominantly distributed in the western areas surrounding Watford, Oil Spring, and Wilikesport (Figure 6b), typically at depths below 250 m, with significant variations in thickness.
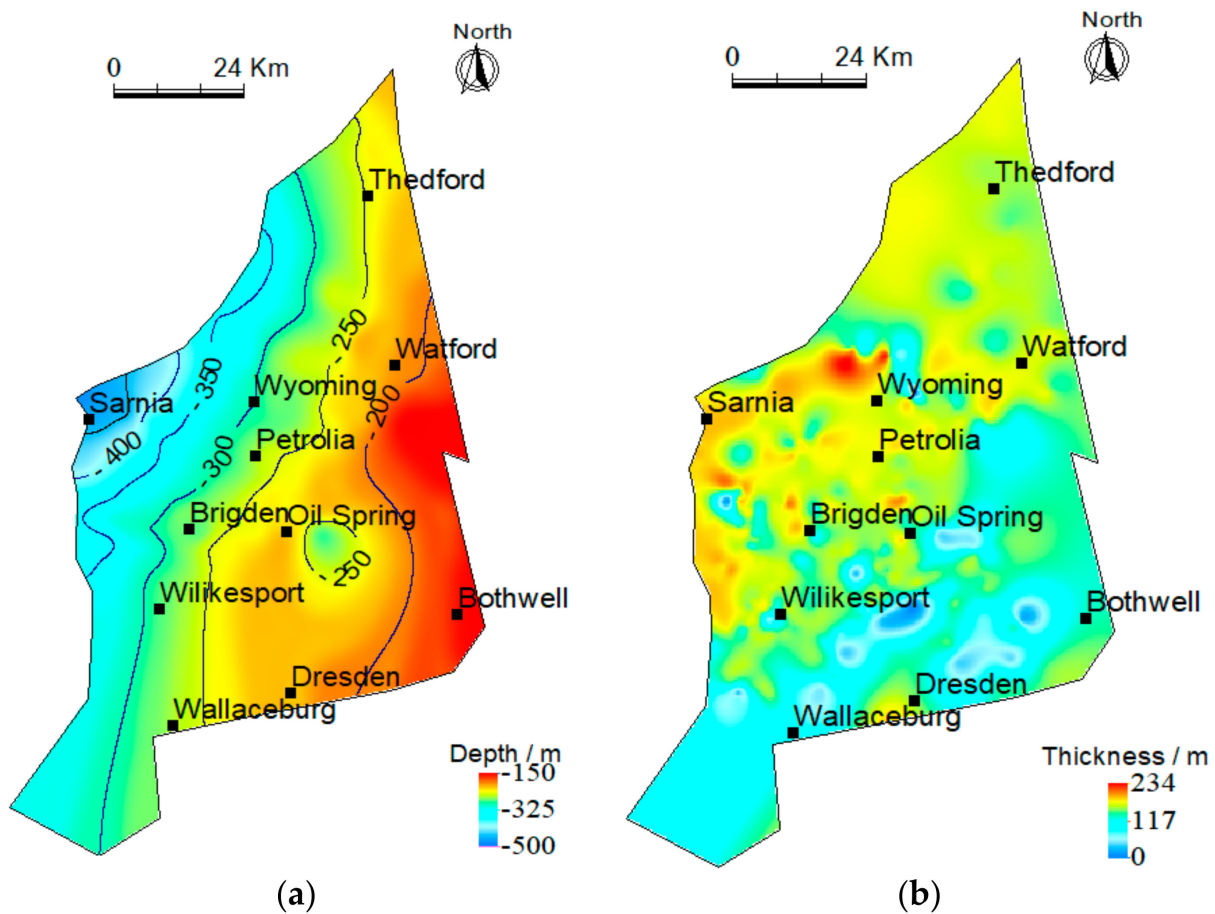


**Figure 6.** The geological characteristics of the B unit in Lambton, Southern Ontario. (**a**) Structural map of the B unit; (**b**) thickness map of the B unit.

## 4.2. The Subunits of the B Unit

Variations in GR and porosity logs (CNL) within the B unit reveal two well-defined sequence boundaries, dividing the B unit into three high-frequency sequence subunits, denoted as SQ1, SQ2, and SQ3 (Figure 7). SQ1 corresponds to salt–limestone in the upper B unit, exhibiting high GR and CNL (Figure 8). SQ2 corresponds to dark bedded salt rocks of the middle B unit. SQ3 consists of massive salt rocks with low GR and CNL. The B unit overlies an anhydrite layer several meters thick, distributed mainly around Wyoming and Brigden.
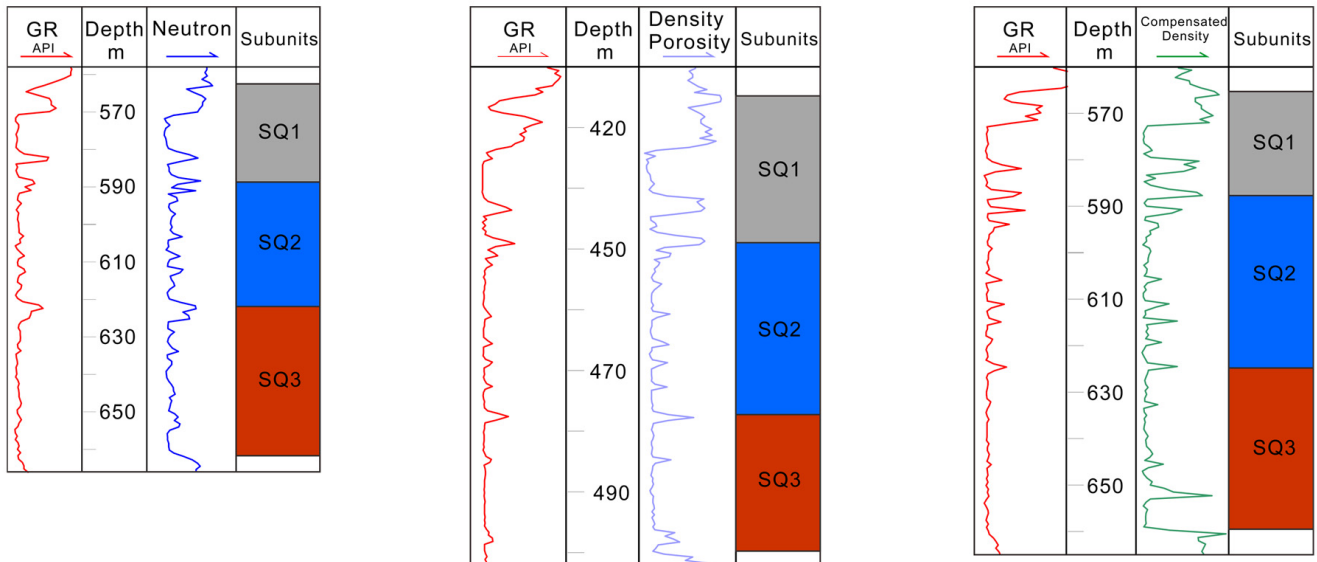


**Figure 7.** The sequence subdivision of the B unit in the T000426, T005758, and T007391 wells based on downhole well logs.
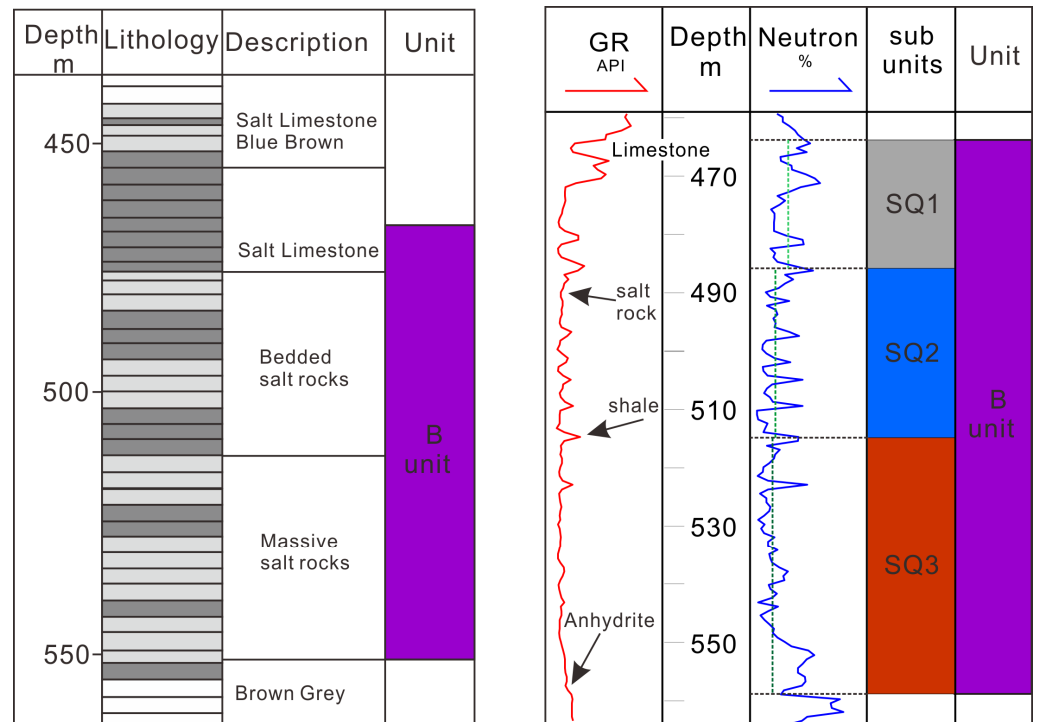


**Figure 8.** The core description and drawings of the F006864 well (**left**) and the well log curves and subunits of the T003039 well (**right**).

## 4.3. The Distribution of Three Subunits

The thickness distribution of SQ1 mirrors that of the B unit, with the thicker sections in the northwest and thinner sections in the southeast (Figure 9a). SQ2 is widespread across the study area except for regions in Petrolia, Brigden, Dresden, and Bothwell (Figure 9b). The distribution of SQ3 is similar to that of SQ2, with thick sections found in the areas of Sarnia, Wyoming, Oil Spring, and Dresden (Figure 9c).
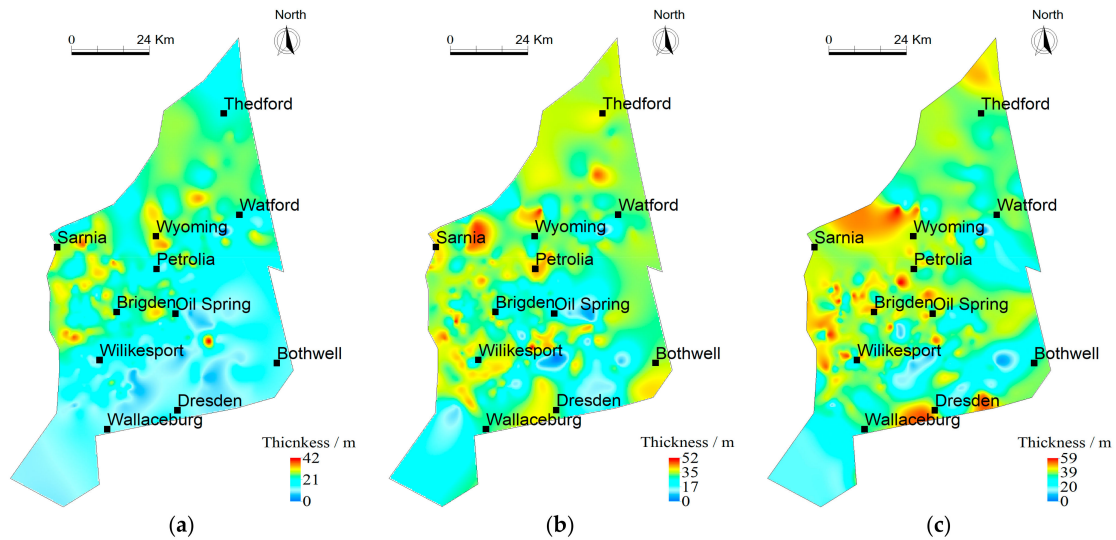


**Figure 9.** The succession thickness map of the three subunits in the B unit. (**a**) SQ1; (**b**) SQ2; (**c**) SQ3.

The spatial form and the thickness of the three subunits indicate the B unit is the combined result of paleogeography, sea-level changes, and tectonic movements. Based on the well log data, simplified paleo-water depth maps of SQ2 and SQ3 were constructed (Figure 10). Paleo-water depth increases northwestward towards the center of the Michigan Basin and deceases southeast towards the axis of the Algonquin Arch, consistent with the regional basin architecture.
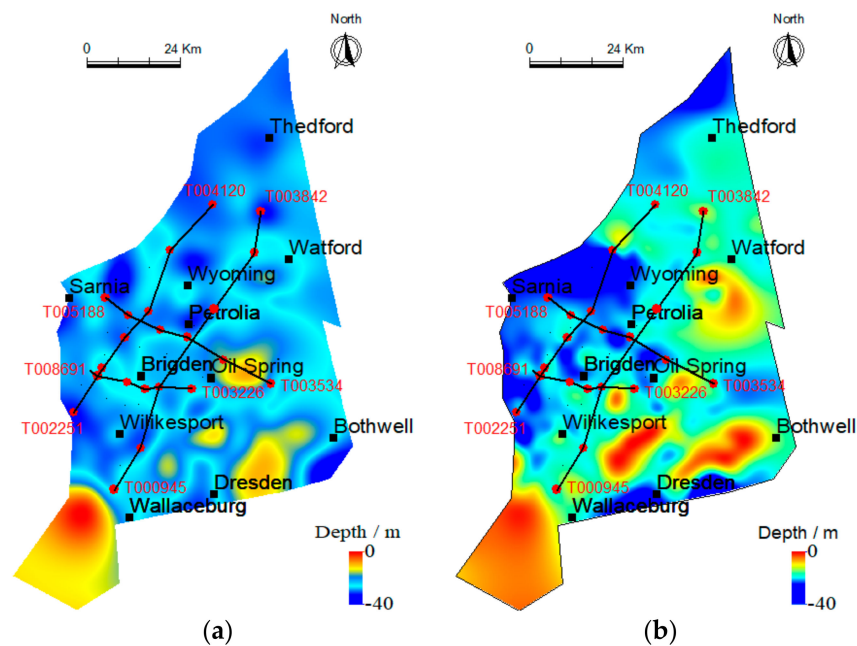


**Figure 10.** The paleogeomorphy maps showing estimated paleo-water depths during the deposition of SQ2 and SQ3. (**a**) SQ2; (**b**) SQ3.

From the cross-sections, the form and thickness of SQ3 are affected by paleogeography or tectonic deformation. SQ3 salt layers are thinner at paleo-highs, around wells T01103 and T006569 in the east–west-running cross-section (Figure 11) and T004120 and T002697 in the north–south-running cross-section (Figure 12). In contrast, SQ2's form and thickness appear relatively consistent across the area, except for wells T003516 and T00945, which show a thickening trend towards the south (Figure 13). SQ1 thins towards the basin margin, particularly in the south and southeast (Figures 9a, 11, 13 and 14).
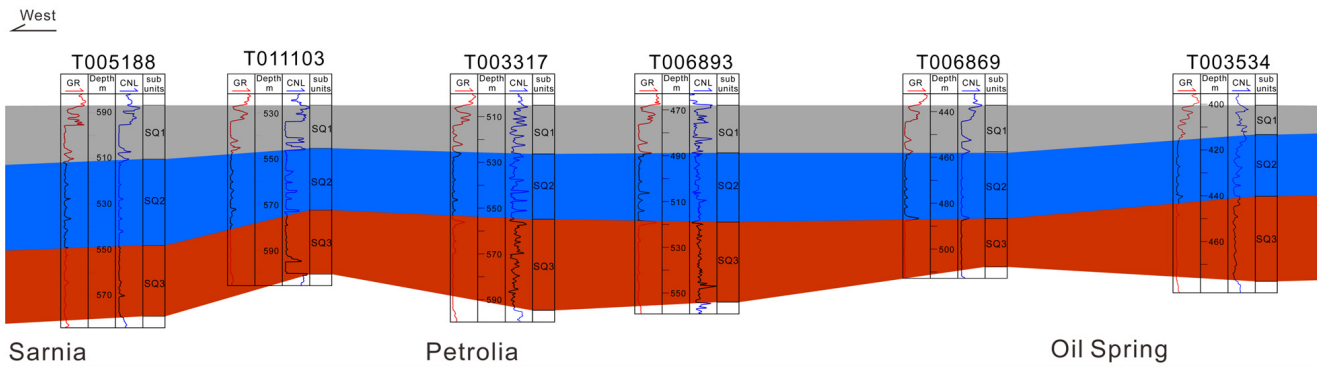


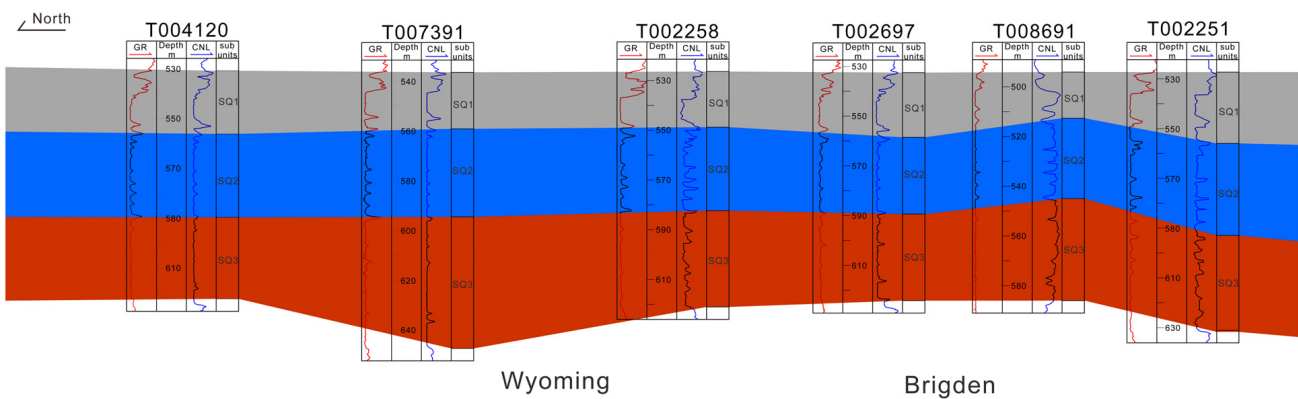**Figure 11.** The well section in the north to south direction in Lambton County.



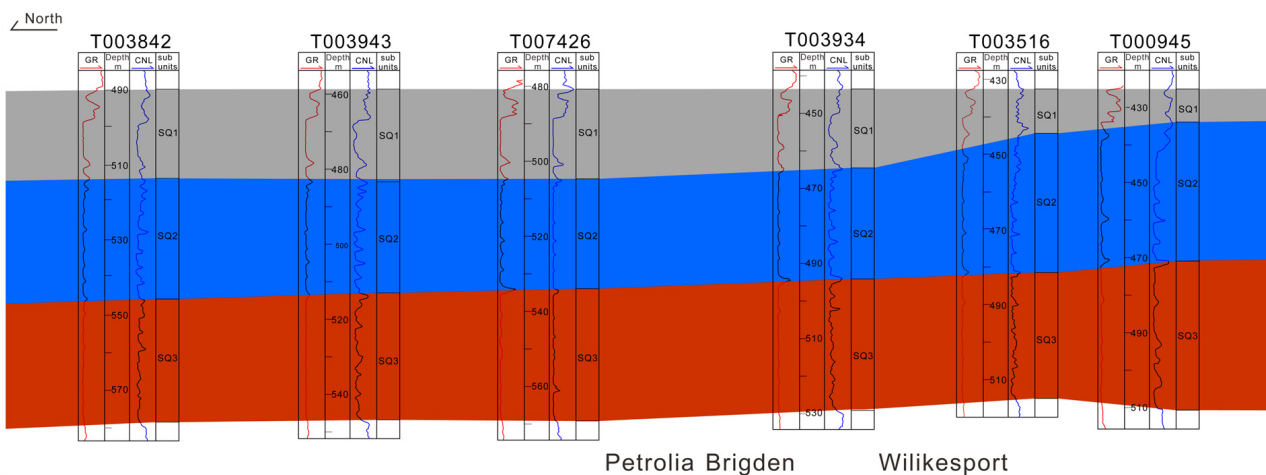**Figure 12.** The well section in the north to south direction in Lambton County.



**Figure 13.** The well section in the north to south direction in Lambton County.
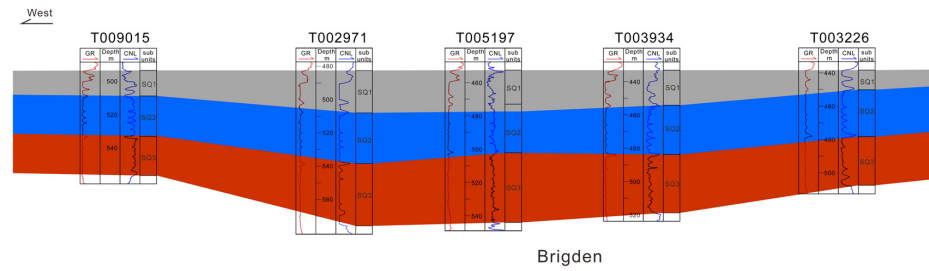
**Figure 14.** The well section around Brigden in the western to eastern direction in Lambton County.

Overall, the study area can be divided into two sub-areas along the Wilikesport, Oil Spring, and Watford line. To the northwest, unit B was thicker and deeper in terms of paleo-water depth, while to the southeast, less of the B unit was deposited on the paleo-highs. Three depositional regions can be identified: one in northern Wyoming, another in a belt around Petrolia, Brigden, and Oil Spring, and a third to the west of Brigden in SQ2 and SQ3.

*4.4. The Potential of Salt Rocks for Energy Storage*

The main thicknesses in SQ1, SQ2, and SQ3 range from 20 to 30 m, 25 to 35 m, and 30 to 40 m, respectively (Figure 15a). SQ1 should be excluded from storage calculations due to its lithology and thickness being economically unviable for cavern development. Therefore, SQ2 and SQ are integrated as a composite unit to represent the B unit for the calculation of storage space. The underground storage volume of salt caverns in the B unit is $9.10 \times 10^6$ m$^3$ (Figure 15b). At the standard state, the working gas volume is $557.80 \times 10^6$ m$^3$ (Figure 15c). The geological storage capacity of salt caverns exhibits significant potential.
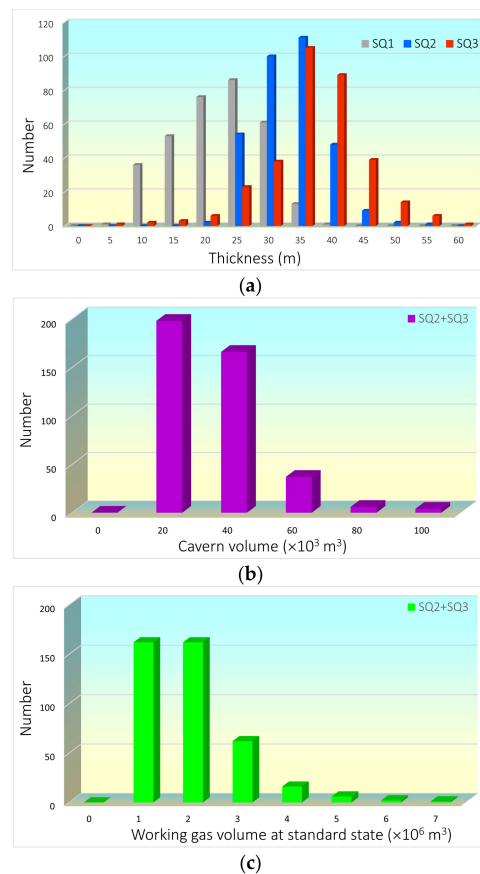


(**a**)



(**b**)



(**c**)

**Figure 15.** The potential of salt rocks for energy storage. (**a**) The thicknesses of the three subunits; (**b**) the volume of salt caverns in SQ2 and SQ3; (**c**) the working gas volume at the standard state in SQ2 and SQ3.

## 5. Discussion

1. The influence of impurity evaporation

An operating cycle in a salt cavern involves injecting, storing, and withdrawing gas. These processes cause fluctuations in pressure and temperature. During an injection/withdrawal cycle, the storage pressure can reach approximately twice the pre-injection pressure, while the temperature can rise by approximately 38 °C [45,46]. These working cycles induce various geomechanical changes, with cavern stability being of the utmost importance. Changes in the working regime can enhance cavern stability, such as by increasing the injection/withdrawal rate and frequency [47,48]. Indeed, the stability of caverns depends on the operating pressure [48,49].

Obviously, cavern pressure affects the surrounding rock to varying extents, primarily because of mechanical property differences caused by rock heterogeneity. Compression tests indicate that the mechanical strength decreases as the impurity content in salt rocks increases, and the brittleness dramatically increases with higher impurity levels [50]. In the B unit, mechanical strength diminishes as the insoluble content rises from SQ3 to SQ1. Mechanical properties in mixed lithotypes depend on the proportion of each end member, with properties nearing those of the dominant end member [51]. The elastic module of halite is smaller than that of anhydrite in bedded salt deposits [51]. This adversely impacts the cavern floor in regions where anhydrite is developed. However, numerical modeling results show a plastic zone developing at the waistline and top of the cavern after 30 years, despite the initial pressure meeting all requirements [48]. The occurrence of plastic zones is likely linked to the fatigue characteristics of the rock, with anhydrite exhibiting higher fatigue strength than halite. Additionally, cracks are another crucial factor that should be considered. Salt rocks containing medium or thicker interlayers show a greater probability of the formation of micro-cracks [52]. Furthermore, a few cracks and fractures appear between the gypsum sheets after hydrogen treatment [53]. It is evident that variations in mechanical properties caused by rock heterogeneity will impact the stability of the cavern.

In unit B, there is a noticeable decrease in homogeneity from SQ3 to SQ1. This change indicates shifts in rock types and physical properties, impacting the safety of underground gas storage in the salt beds. SQ3 consists of pure halite, with low shale content and porosity, and thicker massive salt beds, making it the best subunit for UHS. The secondary subunit is SQ2.

2. The influence of the paleogeography

High confining pressure enhances the mechanical strength of salt rock [54,55]. Variations in confining pressure arise from depth differences within the same subunit. It appears that paleo-water depth correlates with the thickness of the B unit; deeper water corresponds to thicker deposits. This suggests that paleogeography has influenced preferred areas for underground hydrogen storage (UHS). The influence of paleogeography decreases from SQ3 to SQ1. Additionally, paleogeographically controlled differential deposition has led to an uneven distribution of rock thickness. Significant density differences between mudstone and halite create localized variations in the stress field, which, in turn, affect the mechanical performance of salt caverns in depositional areas compared to other regions.

3. The prospecting of geological storage

Thickness maps of the B unit indicate that the favorable area for UHS is around the areas of Wallaceburg, Oil Spring, and Watford in the west (Figure 9b,c). These areas also have high population densities, making them suitable for primary hydrogen resource development. Furthermore, the storage capacity of salt caverns is likely larger than the assessed result due to all wells not being considered. Moreover, the development of three depositional regions and the evolution of in situ stress vary [56]. A more accurate assessment would involve conducting mechanical parameter tests to model the structure of the B unit.

Even if it is not yet time to advance the hydrogen economy system, the substantial subsurface space of the B unit serves various purposes beyond hydrogen storage, such as compressed air storage. Given that hydrogen storage requires high sealing properties of the cap rocks, SQ1 is an ideal candidate for storing other gases, including carbon dioxide.

Underground spaces are increasingly becoming significant emerging resources for energy storage in the transition to a low-carbon economy, necessitating comprehensive assessment.

## 6. Conclusions

1. Vertically, the B unit of the Salina Group can be subdivided into three high-frequency sequence subunits based on variations in lithology and the logging data. The well log corresponding to SQ1 suggests it is an interbedded salt–limestone sequence. Then, SQ2 corresponds to bedded salt with several thin shale layers, and SQ3 corresponds to massive salt rocks.

2. Spatially, the study area can be divided into two sub-areas along the Wilikesport, Oil Spring, and Watford line based on salt thickness and well log characteristics. To the northwest, unit B is thicker and deeper in terms of paleo-water depth, and to the southeast, less of the B unit is deposited on the paleo-highs. The distribution of the B unit and the thickness are controlled jointly by paleogeography, sea-level changes, and tectonic movement in the study area.

3. Lithology (the impurity content of salt rocks) and thickness are two geological factors that influence salt cavern assessment. The best subunit for UHS is SQ3 and the secondary option is SQ2. The lithology and thickness of SQ1 are not favorable for hydrogen storage. The storage capacity of SQ2 is affected by its high mud content, while for SQ3, several meters of anhydrite have developed towards the base of the unit. The favorable area for UHS is the western part of the study area, west of Wallaceburg, Oil Spring, and Watford.

4. The available underground storage volume of the salt caverns in the B unit is $9.10 \times 10^6$ m$^3$. At the standard state, the working gas volume is $557.80 \times 10^6$ m$^3$. The underground storage space of the B unit serves a variety of purposes beyond hydrogen storage. The geological storage capacity of the salt caverns exhibits significant potential. A more accurate assessment would involve conducting mechanical parameter tests to model the structure of the B unit.

**Author Contributions:** Conceptualization, L.L. and S.Y.; methodology, L.L. and S.Y.; investigation, S.Y.; resources, S.Y.; writing—original draft preparation, L.L.; writing—review and editing, S.Y., Z.W. and S.Y. All authors have read and agreed to the published version of the manuscript.

**Data Availability Statement:** The data that support the findings of this study are available from the co-authors upon request.

**Conflicts of Interest:** The authors declare no conflicts of interest.

## References

1. Kabir, M.; Habiba, U.E.; Khan, W.; Shah, A.; Rahim, S.; Rios-Escalante, P.R.D.L.; Farooqi, Z.-U.-R.; Ali, L.; Shafiq, M. Climate Change Due to Increasing Concentration of Carbon Dioxide and Its Impacts on Environment in 21st Century: A Mini Review. *J. King Saud Univ. Sci.* **2023**, *35*, 102693. [CrossRef]
2. Elberry, A.M.; Thakur, J.; Veysey, J. Seasonal Hydrogen Storage for Sustainable Renewable Energy Integration in the Electricity Sector: A Case Study of Finland. *J. Energy Storage* **2021**, *44*, 103474. [CrossRef]
3. Mitali, J.; Dhinakaran, S.; Mohamad, A.A. Energy Storage Systems: A Review. *Energy Storage Sav.* **2022**, *1*, 166–216. [CrossRef]
4. Cheng, W.; Cheng, Y.F. A Techno-Economic Study of the Strategy for Hydrogen Transport by Pipelines in Canada. *J. Pipeline Sci. Eng.* **2023**, *3*, 100112. [CrossRef]
5. Karaca, A.E.; Dincer, I. An Updated Overview of Canada's Hydrogen Related Research and Development Activities. *Int. J. Hydrogen Energy* **2021**, *46*, 34515–34525. [CrossRef]
6. Yuan, S.; Zhu, Y.; Zhao, L.; Liang, S.; Huang, M.; Li, Z. Key Role of Plastic Strain Gradient in Hydrogen Transport in Polycrystalline Materials. *Int. J. Plast.* **2022**, *158*, 103409. [CrossRef]
7. Yu, Y.; Chen, Y.; Jiang, J.; Li, Y. Low-Carbon Scheduling of Integrated Hydrogen Transport and Energy System. *Int. J. Hydrogen Energy* **2024**, *52*, 655–666. [CrossRef]

8.  Sambo, C. A Review on Worldwide Underground Hydrogen Storage Operating and Potential Fields. *Int. J. Hydrogen Energy* **2022**, *47*, 22840–22880. [CrossRef]

9.  Petrillo, A.; Felice, F.D.; Jannelli, E.; Minutillo, M. Chapter 5—Life Cycle Cost Analysis of Hydrogen Energy Technologies. In *Hydrogen Economy*; Scipioni, A., Manzardo, A., Ren, J., Eds.; Academic Press: New York, NY, USA, 2017; pp. 121–138.

10. Bünger, U.; Michalski, J.; Crotogino, F.; Kruck, O. 7—Large-Scale Underground Storage of Hydrogen for the Grid Integration of Renewable Energy and Other Applications. In *Compendium of Hydrogen Energy*; Ball, M., Basile, A., Veziroğlu, T.N., Eds.; Woodhead Publishing Series in Energy; Woodhead Publishing: Oxford, UK, 2016; pp. 133–163.

11. Panfilov, M. 4—Underground and Pipeline Hydrogen Storage. In *Compendium of Hydrogen Energy*; Gupta, R.B., Basile, A., Veziroğlu, T.N., Eds.; Woodhead Publishing Series in Energy; Woodhead Publishing: Oxford, UK, 2016; pp. 91–115.

12. Koholé, Y.W.; Wankouo Ngouleu, C.A.; Fohagui, F.C.V.; Tchuen, G. A Comprehensive Comparison of Battery, Hydrogen, Pumped-Hydro and Thermal Energy Storage Technologies for Hybrid Renewable Energy Systems Integration. *J. Energy Storage* **2024**, *93*, 112299. [CrossRef]

13. Gasanzade, F.; Pfeiffer, W.T.; Witte, F.; Tuschy, I.; Bauer, S. Subsurface Renewable Energy Storage Capacity for Hydrogen, Methane and Compressed Air—A Performance Assessment Study from the North German Basin. *Renew. Sustain. Energy Rev.* **2021**, *149*, 111422. [CrossRef]

14. Thomas, K.M. Hydrogen Adsorption and Storage on Porous Materials. *Catal. Today* **2007**, *120*, 389–398. [CrossRef]

15. Hirscher, M.; Yartys, V.A.; Baricco, M.; Bellosta von Colbe, J.; Blanchard, D.; Bowman, R.C.; Broom, D.P.; Buckley, C.E.; Chang, F.; Chen, P.; et al. Materials for Hydrogen-Based Energy Storage—Past, Recent Progress and Future Outlook. *J. Alloys Compd.* **2020**, *827*, 153548. [CrossRef]

16. Wallace, R.L. Utility-Scale Subsurface Hydrogen Storage: UK Perspectives and Technology. *Int. J. Hydrogen Energy* **2021**, *46*, 25137–25159. [CrossRef]

17. Michalski, J.; Bünger, U.; Crotogino, F.; Donadei, S.; Schneider, G.-S.; Pregger, T.; Cao, K.-K.; Heide, D. Hydrogen Generation by Electrolysis and Storage in Salt Caverns: Potentials, Economics and Systems Aspects with Regard to the German Energy Transition. *Int. J. Hydrogen Energy* **2017**, *42*, 13427–13443. [CrossRef]

18. Kabuth, A.; Dahmke, A.; Beyer, C.; Bilke, L.; Dethlefsen, F.; Dietrich, P.; Duttmann, R.; Ebert, M.; Feeser, V.; Görke, U.-J.; et al. Energy Storage in the Geological Subsurface: Dimensioning, Risk Analysis and Spatial Planning: The ANGUS+ Project. *Environ. Earth Sci.* **2017**, *76*, 23. [CrossRef]

19. Bartel, S.; Janssen, G. Underground Spatial Planning—Perspectives and Current Research in Germany. *Tunn. Undergr. Space Technol.* **2016**, *55*, 112–117. [CrossRef]

20. Bennion, D.B.; Thomas, F.B.; Ma, T.; Imer, D. Detailed Protocol for the Screening and Selection of Gas Storage Reservoirs. In *All Days*; SPE: Calgary, AB, Canada, 2000; p. SPE-59738-MS.

21. Lankof, L.; Urbańczyk, K.; Tarkowski, R. Assessment of the Potential for Underground Hydrogen Storage in Salt Domes. *Renew. Sustain. Energy Rev.* **2022**, *160*, 112309. [CrossRef]

22. Lankof, L. Assessment of the Potential for Underground Hydrogen Storage in Bedded Salt Formation. *Int. J. Hydrogen Energy* **2020**, *45*, 19479–19492. [CrossRef]

23. Lemieux, A.; Shkarupin, A.; Sharp, K. Geologic Feasibility of Underground Hydrogen Storage in Canada. *Int. J. Hydrogen Energy* **2020**, *45*, 32243–32259. [CrossRef]

24. IESO. Imports and Exports. Available online: https://www.ieso.ca/Power-Data/Supply-Overview/Imports-and-Exports (accessed on 9 July 2024).

25. Ohta, S. Molecular Hydrogen as a Preventive and Therapeutic Medical Gas: Initiation, Development and Potential of Hydrogen Medicine. *Pharmacol. Ther.* **2014**, *144*, 1–11. [CrossRef]

26. Habib, M.A.; Abdulrahman, G.A.Q.; Alquaity, A.B.S.; Qasem, N.A.A. Hydrogen Combustion, Production, and Applications: A Review. *Alex. Eng. J.* **2024**, *100*, 182–207. [CrossRef]

27. Liu, H.; Almansoori, A.; Fowler, M.; Elkamel, A. Analysis of Ontario's Hydrogen Economy Demands from Hydrogen Fuel Cell Vehicles. *Int. J. Hydrogen Energy* **2012**, *37*, 8905–8916. [CrossRef]

28. Lemieux, A.; Sharp, K.; Shkarupin, A. Preliminary Assessment of Underground Hydrogen Storage Sites in Ontario, Canada. *Int. J. Hydrogen Energy* **2019**, *44*, 15193–15204. [CrossRef]

29. Armstrong, D.K.; Carter, T.R. *An Updated Guide to the Subsurface Paleozoic Stratigraphy of Southern Ontario*; Open File Report 6191; Ontario Geological Survey: Toronto, ON, Canada, 2006.

30. Hui, S.; Yin, S.; Pang, X.; Chen, Z.; Shi, K. Potential of Salt Caverns for Hydrogen Storage in Southern Ontario, Canada. *Mining* **2023**, *3*, 399–408. [CrossRef]

31. Al-Yaseri, A.; Al-Mukainah, H.; Yekeen, N.; Al-Qasim, A.S. Experimental Investigation of Hydrogen-Carbonate Reactions via Computerized Tomography: Implications for Underground Hydrogen Storage. *Int. J. Hydrogen Energy* **2023**, *48*, 3583–3592. [CrossRef]

32. Minougou, J.D.; Gholami, R.; Andersen, P. Underground Hydrogen Storage in Caverns: Challenges of Impure Salt Structures. *Earth-Sci. Rev.* **2023**, *247*, 104599. [CrossRef]

33. Mansour, A.; Adeyilola, A.; Gentzis, T.; Carvajal-Ortiz, H.; Zakharova, N. Depositional Setting and Organic Matter Characterization of the Upper Devonian Antrim Shale, Michigan Basin: Implications for Hydrocarbon Potential. *Mar. Pet. Geol.* **2022**, *140*, 105683. [CrossRef]

34. Rine, M.J.; McLaughlin, P.I.; Bancroft, A.M.; Harrison, W.B.; Kuglitsch, J.; Caruthers, A.H.; Ramezani, J.; Kaczmarek, S.E.; Emsbo, P. Linked Silurian Carbon Cycle Perturbations, Bursts of Pinnacle Reef Growth, Extreme Sea-Level Oscillations, and Evaporite Deposition (Michigan Basin, USA). *Palaeogeogr. Palaeoclimatol. Palaeoecol.* **2020**, *554*, 109806. [CrossRef]

35. Al-Aasm, I.S.; Crowe, R. Fluid Compartmentalization and Dolomitization in the Cambrian and Ordovician Successions of the Huron Domain, Michigan Basin. *Mar. Pet. Geol.* **2018**, *92*, 160–178. [CrossRef]

36. Beauheim, R.L.; Roberts, R.M.; Avis, J.D. Hydraulic Testing of Low-Permeability Silurian and Ordovician Strata, Michigan Basin, Southwestern Ontario. *J. Hydrol.* **2014**, *509*, 163–178. [CrossRef]

37. Mesolella, K.J.; Robinson, J.D.; McCormick, L.M.; Ormiston, A.R. Cyclic Deposition of Silurian Carbonates and Evaporites in Michigan Basin. *AAPG Bull.* **1974**, *58*, 34–62.

38. Sonnenfeld, P.; Al-Aasm, I. The Salina Evaporites in the Michigan Basin. In *Early Sedimentary Evolution of the Michigan Basin*; Catacosinos, P.A., Daniels, P.A., Jr., Eds.; Geological Society of America: Boulder, CO, USA, 1991; Volume 256.

39. Hemenway, M.A.; Kaczmarek, S.E. High-Resolution Chemostratigraphy in Carbonate Mudstones: Salina A-1 Carbonate (Silurian), Michigan Basin, U.S.A. *Mar. Pet. Geol.* **2021**, *126*, 104918. [CrossRef]

40. Kansas Geological Survey. Geological Log Analysia. Available online: https://www.kgs.ku.edu/Publications/Bulletins/LA/07 _evaporites.html (accessed on 9 July 2024).

41. Coianiz, L.; Bialik, O.M.; Ben-Avraham, Z.; Lazar, M. Late Quaternary Lacustrine Deposits of the Dead Sea Basin: High Resolution Sequence Stratigraphy from Downhole Logging Data. *Quat. Sci. Rev.* **2019**, *210*, 175–189. [CrossRef]

42. Williams, J.D.O.; Williamson, J.P.; Parkes, D.; Evans, D.J.; Kirk, K.L.; Sunny, N.; Hough, E.; Vosper, H.; Akhurst, M.C. Does the United Kingdom Have Sufficient Geological Storage Capacity to Support a Hydrogen Economy? Estimating the Salt Cavern Storage Potential of Bedded Halite Formations. *J. Energy Storage* **2022**, *53*, 105109. [CrossRef]

43. Parkes, D.; Evans, D.J.; Williamson, P.; Williams, J.D.O. Estimating Available Salt Volume for Potential CAES Development: A Case Study Using the Northwich Halite of the Cheshire Basin. *J. Energy Storage* **2018**, *18*, 50–61. [CrossRef]

44. Evans, D.; Parkes, D.; Dooner, M.; Williamson, P.; Williams, J.; Busby, J.; He, W.; Wang, J.; Garvey, S. Salt Cavern Exergy Storage Capacity Potential of UK Massively Bedded Halites, Using Compressed Air Energy Storage (CAES). *Appl. Sci.* **2021**, *11*, 4728. [CrossRef]

45. Caglayan, D.G.; Weber, N.; Heinrichs, H.U.; Linßen, J.; Robinius, M.; Kukla, P.A.; Stolten, D. Technical Potential of Salt Caverns for Hydrogen Storage in Europe. *Int. J. Hydrogen Energy* **2020**, *45*, 6793–6805. [CrossRef]

46. Ruiz Maraggi, L.M.; Moscardelli, L.G. Modeling Hydrogen Storage Capacities, Injection and Withdrawal Cycles in Salt Caverns: Introducing the GeoH2 Salt Storage and Cycling App. *Int. J. Hydrogen Energy* **2023**, *48*, 26921–26936. [CrossRef]

47. Liu, W.; Duan, X.; Li, Q.; Wan, J.; Zhang, X.; Fang, J.; Jiang, D.; Chen, J. Analysis of Pressure Interval/Injection and Production Frequency on Stability of Large-Scale Supercritical $CO_2$ Storage in Salt Caverns. *J. Clean. Prod.* **2023**, *433*, 139731. [CrossRef]

48. Liu, W.; Dong, Y.; Zhang, Z.; Li, L.; Jiang, D.; Fan, J.; Chen, J.; Zhang, X.; Wan, J.; Li, Z. Optimization of Operating Pressure of Hydrogen Storage Salt Cavern in Bedded Salt Rock with Multi-Interlayers. *Int. J. Hydrogen Energy* **2024**, *58*, 974–986. [CrossRef]

49. Cyran, K.; Kowalski, M. Shape Modelling and Volume Optimisation of Salt Caverns for Energy Storage. *Appl. Sci.* **2021**, *11*, 423. [CrossRef]

50. Liu, W.; Zhang, X.; Fan, J.; Zuo, J.; Zhang, Z.; Chen, J. Study on the Mechanical Properties of Man-Made Salt Rock Samples with Impurities. *J. Nat. Gas Sci. Eng.* **2020**, *84*, 103683. [CrossRef]

51. Liang, W.; Yang, C.; Zhao, Y.; Dusseault, M.B.; Liu, J. Experimental Investigation of Mechanical Properties of Bedded Salt Rock. *Int. J. Rock Mech. Min. Sci.* **2007**, *44*, 400–411. [CrossRef]

52. Li, Y.; Liu, W.; Yang, C.; Daemen, J.J.K. Experimental Investigation of Mechanical Behavior of Bedded Rock Salt Containing Inclined Interlayer. *Int. J. Rock Mech. Min. Sci.* **2014**, *69*, 39–49. [CrossRef]

53. Fatah, A.; Al-Yaseri, A.; Theravalappil, R.; Radwan, O.A.; Amao, A.; Al-Qasim, A.S. Geochemical Reactions and Pore Structure Analysis of Anhydrite/Gypsum/Halite Bearing Reservoirs Relevant to Subsurface Hydrogen Storage in Salt Caverns. *Fuel* **2024**, *371*, 131857. [CrossRef]

54. Lyu, C.; Liu, J.; Ren, Y.; Liang, C.; Zeng, Y. Mechanical Characteristics and Permeability Evolution of Salt Rock under Thermal-Hydro-Mechanical (THM) Coupling Condition. *Eng. Geol.* **2022**, *302*, 106633. [CrossRef]

55. Han, Y.; Ma, H.; Yang, C.; Li, H.; Yang, J. The Mechanical Behavior of Rock Salt under Different Confining Pressure Unloading Rates during Compressed Air Energy Storage (CAES). *J. Pet. Sci. Eng.* **2021**, *196*, 107676. [CrossRef]

56. Howell, P.D.; Van Der Pluijm, B.A. Structural Sequences and Styles of Subsidence in the Michigan Basin. *Geol. Soc. Am. Bull.* **1999**, *111*, 974–991. [CrossRef]